Enhancing Power Harvesting Using a Tuned Auxiliary Structure

Michael Damianakis[1], Jan Goethals[2], Jeffrey Kowtko[3], Phillip Cornwell[4]

[1]Undergraduate, Dept. of Mechanical Eng., Georgia Institute of Technology, Atlanta, GA 30332
[2]Graduate, Dept. of Civil Eng., Univ. of California at Berkeley, Berkeley, CA 94704
[3]Graduate, Dept. of Aerospace Eng., Univ. of Illinois at Urbana-Champaign, Urbana-Champaign, IL 61801
[4]Professor of Mechanical Engineering, Rose-Hulman Institute of Technology, Terre Haute, IN 47803

ABSTRACT

In the future, self-contained sensors and processing units will need on-board, renewable power supplies to be truly autonomous. One way of supplying such power is through energy harvesting, a process by which ambient forms of energy are converted into electricity. One energy harvesting technique involves converting kinetic energy, in the form of vibrations, into electrical energy through the use of piezoelectric materials. This study examines the use of auxiliary structures, consisting of a mechanical fixture and a lead zirconate/lead titanate (PZT) piezoelectric element, which can be attached to any vibrating system. Adjusting various parameters of these structures can maximize the strain induced in the attached PZT element and improve power output.

NOMENCLATURE

b	width of PZT patch	p_i	principle coordinate of the i^{th} mode
C_i	modal damping of the i^{th} mode	q	charge
C_p	capacitance of PZT patch	R	radius of curvature
D_n	electrical displacement along direction n of PZT	T_n	stress in direction n
d_{nm}	strain constant	t_p	thickness of PZT patch
E	elastic modulus of the auxiliary structure	t	thickness of the auxiliary structure
E_p	elastic modulus of PZT patch	V_{out}	PZT voltage output
g_{nm}	voltage constant (voltage in direction n / stress in direction m)	y'	slope of auxiliary structure (dy/dx)
I	area moment of inertia of the auxiliary structure	y_a	displacement in y direction at end of cantilevered beam
j	$\sqrt{-1}$	y_c	distance from neutral axis of PZT
K_a	stiffness of auxiliary structure	y_m	displacement of host structure at the location of the auxiliary structure
K_i	modal stiffness of the i^{th} mode	$[M]$	mass matrix
K_s	term reduction, see equation 4	$[C]$	damping matrix
L	length of the auxiliary structure	$[K]$	stiffness matrix
L_p	length of PZT patch	$\{F\}$	forcing vector
M	point mass	$\{p\}$	vector of principal coordinates
M_a	mass of the auxiliary structure	$[\Phi]$	modal matrix
M_i	modal mass of the i^{th} mode	ϕ_{ik}	modal matrix, k^{th} element of the i^{th} mode
M_b	mass of the auxiliary structure (excluding point mass)	ω	angular frequency

1. INTRODUCTION

Researchers are currently investigating how piezoelectric materials can be used to harvest power. Advances in low power sensing and computing have provided a major impetus for this work. Power requirements for wireless sensors, digital signal processors, and wireless communication devices have been reduced to the range of tens to hundreds of microwatts [1]. This power reduction allows new possibilities for various applications, including structural health monitoring and damage prognosis [2]. By eliminating the need for power transmission wires, structures can be monitored with autonomous, self-contained sensor systems. A possible solution to the problem of localized power generation includes developing technologies that enable harvesting of ambient energy [3,4]. Forms of energy that may be harvested include thermal, mechanical, acoustic, and solar. Batteries have the potential to provide long lasting power; however, they are unreliable and eventually require maintenance. If power can be supplied by ambient sources, the sensor system can potentially operate indefinitely [5]. Several researchers have demonstrated harvesting power from ambient motion [6,7]. Starner verified that walking and other human functions, such as arm motion, could be used to power a computer [6]. Elvin et. al. used a polyvinyl difluoride (PVDF) membrane as a self-powered strain energy sensor capable of detecting damage and transmitting data wirelessly to a remote receiver [7,8].

A number of researchers have worked on quantifying the performance of PZT power harvesting systems [4, 9]. In Roundy et. al., two piezoelectric patches were attached to a steel cantilevered beam and used to collect mechanical energy from vibrations to be used as a power source for wireless sensor nodes. By using an excitation force designed to simulate the vibration of an operating microwave oven, the piezoelectric material achieved a 70 $\mu W/cm^3$ power density [9]. Sodano et. Al. estimated the power output from a PZT cantilever auxiliary structure attached to an automobile compressor. A 40 mm by 62 mm PSI-5H4E PZT from Piezo Systems Inc. mounted to a fixed-free, 40 mm by 80 mm plate was able to charge a 40 mAh button cell battery in one hour [4].

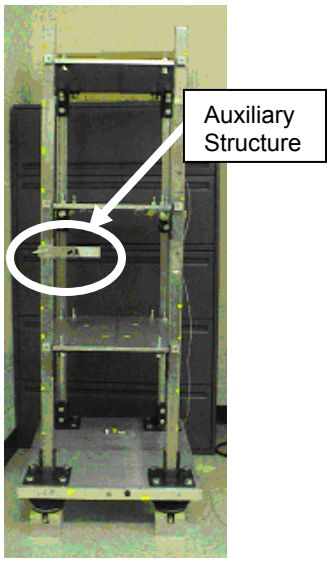

Figure 1: Photograph of the three-story frame structure and the auxiliary cantilever beam

Several studies have examined optimizing power harvesting by using a DC-DC converter [10,11], that is, by modifying the electrical circuit used in power harvesting, but to date no studies have examined how to increase the power available from the PZT using a tuned auxiliary structure. In this study, the concept of attaching a tuned auxiliary structure, basically a vibration absorber, to a host structure to enhance power harvesting was investigated. A beam was attached to a three-story frame structure as shown in Figure 1. Identical PZT patches were attached to the host structure and to the auxiliary structure and the maximum power output was compared. An equation to relate modal characteristics of the host structure, piezoelectric properties and the auxiliary structure's geometry and location to PZT voltage output was developed. Experiments were conducted to validate the relationships developed from the theory.

Two primary design considerations were investigated: (1) the location of the auxiliary structure on the host structure, and (2) the frequency to which the auxiliary structure was tuned.

2. THEORY

A schematic of the auxiliary structure used in this study is shown in Figure 2. In this section, the expected output voltage of the PZT patch is derived assuming the first bending mode of the auxiliary structure is tuned to one of the natural modes of the host structure.

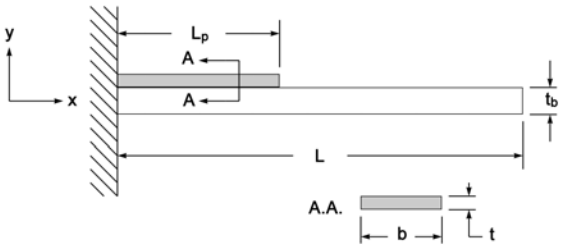

Figure 2: Schematic of cantilevered beam mount

The electrical displacement of a PZT patch, $D_3(x,y)$ with no electric field applied is defined to be

$$D_3(x,y) = d_{31}T_1(x,y) \tag{1}$$

where d_{31} is a strain constant for the PZT material and T(x,y) is the stress [12]. By taking the average stress at the centroidal axis of the PZT patch (distance y_c from the neutral axis), the dependence on y can be eliminated from the equation

$$D_3(x) = d_{31}T_1(x,y_c) = d_{31}\frac{y_c E_p}{R} \cong d_{31}y_c E_p \frac{d^2y}{dx^2} \tag{2}$$

where E_p is the Young's Modulus for the PZT material and R is the radius of curvature at x. Eq. (2) assumes small deflections. The charge, q, at the poles of the sensor can be determined by integrating over the area of the PZT sensor, that is,

$$\begin{aligned} q &= \int_A \boldsymbol{D}\cdot\boldsymbol{n}dA = \int_0^{L_p} d_{31}y_c E_p \frac{d^2y}{dx^2} b dx \\ &= d_{31}y_c E_p b\left(y'(L_p) - y'(0)\right) = d_{31}y_c E_p b y'(L_p) \end{aligned} \tag{3}$$

The PZT output voltage is calculated by dividing the charge given in Eq. (3) by the capacitance of the PZT, C_p, as shown in Eq. (4),

$$V_{out}(t) = \frac{q}{C_p} = \frac{d_{31}y_c E_p b}{C_p} y'(L_p) = K_s y'(L_p) \tag{4}$$

where K_s depends on the properties and geometry of the PZT. This relationship reveals that the output voltage is a function of K_s and the slope of the PZT at the end furthest from the base of the cantilever. To determine the slope of the PZT, an expression for the slope of the auxiliary structure is derived in terms of displacement at the end of a cantilevered beam, $y(L)\equiv y_a$. Assuming a static point load at the end of a cantilever beam, the slope can be expressed in terms of the displacement at the end of the beam [13]

$$y'(x) = \frac{3y_a}{2L^3}\left(2Lx - x^2\right) \tag{5}$$

Note that the relationship of the tip displacement to the slope could have been determined assuming a distributed load or even by using the exact shape of the first bending mode of a beam, but the slope does not change significantly and the general trends are the same. The point load displacement was used since it results in the simplest equation. Letting $x = L_p$, that is evaluating the slope at the end of the PZT patch, and substituting Eq. (5) into Eq. (4) gives

$$V_{out}(t) = \frac{3K_s y_a}{2L^3}\left(2LL_p - L_p^2\right) \tag{6}$$

According to Eq. (6), the output voltage will be largest if the PZT is the same length as the beam. This result assumes the structure has a displacement field very similar to its first bending mode. Clearly, in the actual structure this will not necessarily be the case due to the effect of higher frequency modes. The motion of the auxiliary structure and of the host structure will dictate the displacement at the end of the cantilevered beam, y_a. To better understand this motion, a single-degree-of-freedom (SDOF) model can be developed for the host structure. The host structure being examined can be modeled as a general multi-degree-of-freedom system

$$[M]\{\ddot{y}\} + [C]\{\dot{y}\} + [K]\{y\} = \{F(t)\} \tag{7}$$

where [M], [C], and [K] are the system mass, damping and stiffness matrices respectively, and {F} is the forcing vector. If the forcing is only applied to the k^{th} degree-of-freedom then

$$\{F\}^T = \left\{ 0 \quad 0 \ \ldots \ 0 \quad \underbrace{F(t)}_{k^{th}\text{element of } \{F\}} \quad 0 \ \ldots \ 0 \quad 0 \right\} \tag{8}$$

Assuming the modal matrix for this structure is $[\Phi]$, a transformation of coordinates can be used to decouple these equations

$$\{y\} = [\Phi]\{p\} \tag{9}$$

where {*p*} are principle coordinates. Substituting Eq. (9) into Eq. (7) and multiplying by $[\Phi]^T$ gives

$$[\Phi]^T [M][\Phi]\{\ddot{p}\} + [\Phi]^T [C][\Phi]\{\dot{p}\} + [\Phi]^T [K][\Phi]\{p\} = [\Phi]^T \{F(t)\} \tag{10}$$

Using the fact that the modes, i.e. the eigenvectors, are orthogonal with respect to the mass and stiffness matrix, and assuming proportional damping, Eq. (10) reduces to a set of decoupled equations

$$M_i \ddot{p}_i + C_i \dot{p}_i + K_i p_i = \phi_{ik} F \tag{11}$$

where M_i, C_i, and K_i are the modal mass, damping and stiffness respectively for the ith mode and ϕ_{ik} is the kth element of the ith mode. To design a vibration absorber for this system it is assumed that only one mode, denoted by the subscript n, of the structure is excited. Therefore, Eq. (11) becomes

$$M_n \ddot{p}_n + C_n \dot{p}_n + K_n p_n = \phi_{nk} F \tag{12}$$

where ϕ_{nk} is the kth element of the nth mode and is an indication of how well mode n will be excited by {F}. Eq. (12) is written in terms of principle coordinates. To write the coupled equations of motion between the vibration absorber and the structure, Eq. (12) needs to be written in terms of the displacement at the DOF where the absorber is attached to the host structure. This DOF is defined to be y_m. From Eq. (9)

$$y_m = \phi_{na} p_n \tag{13}$$

where ϕ_{na} is the magnitude of the nth mode at the location of the auxiliary structure. Solving Eq. (13) for p_n and substituting into Eq. (12) gives

$$M_n \frac{\ddot{y}_m}{\phi_{na}} + C_n \frac{\dot{y}_m}{\phi_{na}} + K_n \frac{y_m}{\phi_{na}} = \phi_{nk} F \tag{14}$$

Multiplying through by ϕ_{na} gives a SDOF structural vibration model at a single mode n

$$M_n \ddot{y}_m + C_n \dot{y}_m + K_n y_m = \phi_{na}\phi_{nk} F \tag{15}$$

The auxiliary structure is attached to the host structure and is designed to be a vibration absorber. As Figure 3 shows, this arrangement can be represented as a two-degree-of-freedom (2DOF) system. Damping of the auxiliary structure is not accounted for, because it is assumed to be small. The coupled equations of motion for the system shown in Figure 3 are:

$$M_n \ddot{y}_m + C_n \dot{y}_m + (K_n + K_a) y_m - K_a y_a = \phi_{na}\phi_{nk} F \tag{16}$$

$$M_a \ddot{y}_a + K_a y_a - K_a y_m = 0 \tag{17}$$

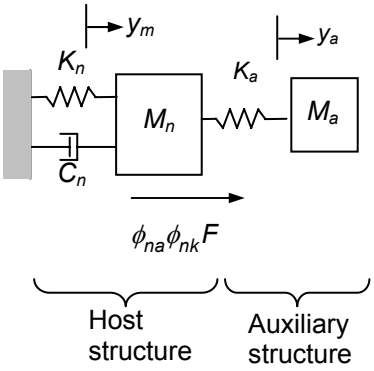

Figure 3: Host structure and auxiliary structure modeled as a 2 DOF system

By using the Fourier Transform with zero initial conditions, Eq. (16) and (17) can be written in the frequency domain as

$$\begin{bmatrix} K_n + K_a - M_n\omega^2 + j\omega C_n & -K_a \\ -K_a & K_a - M_a\omega^2 \end{bmatrix} \begin{bmatrix} Y_m \\ Y_a \end{bmatrix} = \begin{bmatrix} \phi_{na}\phi_{nk}F(\omega) \\ 0 \end{bmatrix} \tag{18}$$

Solving for the displacements gives

$$\begin{bmatrix} Y_m \\ Y_a \end{bmatrix} = \frac{\begin{bmatrix} K_a - M_a\omega^2 & K_a \\ K_a & K_n + K_a - M_n\omega^2 + j\omega C_n \end{bmatrix}}{\Delta(\omega)} \begin{bmatrix} \phi_{na}\phi_{nk}F(\omega) \\ 0 \end{bmatrix} = \begin{bmatrix} \frac{K_a - M_a\omega^2}{\Delta(\omega)}\phi_{na}\phi_{nk}F(\omega) \\ \frac{K_a}{\Delta(\omega)}\phi_{na}\phi_{nk}F(\omega) \end{bmatrix} \tag{19}$$

where $\Delta(\omega) = \left(K_n + K_a - M_n\omega^2 + j\omega C_n\right)\left(K_a - M_a\omega^2\right) - K_a^2$. Choosing $\omega^2 = K_a/M_a$ we can minimize Y_m and maximize Y_a, that is, $Y_m = 0$ and the displacement of the auxiliary structure at its tip is

$$y_a = \frac{-\phi_{na}\phi_{nk}F}{K_a} = \frac{-\phi_{na}\phi_{nk}FL^3}{3EI} \tag{20}$$

The negative sign in Eq. (20) simply indicates that the force, F, and displacement, y_a, are 180 degrees out of phase with each other. Substituting the magnitude of the tip displacement, y_a, into Eq. (6) gives

$$V_{out}(t) = \frac{K_s\phi_{na}\phi_{nk}F}{2EI}\left(2LL_p - L_p^2\right) \tag{21}$$

Eq. (21) reveals the significant parameters that affect the system's ability to produce output voltage and provides the necessary design considerations. The factor ϕ_{na} is the magnitude of the nth mode at the location of the auxiliary structure. In order to increase the output voltage, the placement of the auxiliary structure should be selected such that the magnitude of the nth mode is largest in that location. If the auxiliary structure happens to rest on a node of the particular mode, little or no power will be harvested if the auxiliary structure is tuned to that mode. A modal test can be used to identify the nodes and antinodes of the modes of interest. The factor ϕ_{nk} accounts for the input force location. Depending on the location of the force input, the modes will be excited differently. If there is ample energy in the tuned mode given an experimental force input, but virtually no energy given the input seen under normal operating conditions, then there would not be substantial voltage output during operation. For this reason it is critical that the true force input is used when selecting the mode to tune for. The output voltage is also directly proportional to the forcing function. If the force to the system is increased, the force response is increased uniformly across all the modes. For any possible mode, and at any possible location, barring nodes, the voltage will increase.

Another relationship that can be observed from Eq. (21) is how the material and geometric properties of the auxiliary structure affect the voltage output of the attached PZT. A higher elastic modulus and moment of inertia for the auxiliary beam will effectively reduce the deflection of the beam, and consequently the stress in the PZT. For a given size of PZT, the length of the auxiliary structure should be maximized with the constraint that it still be tuned to the desired natural frequency of the host structure.

3. EXPERIMENT AND MODEL SETUP

The test structure, shown in Figure 4, models a three-story moment resisting frame. The columns are aluminum Unistruts and the floor plates are 1.3 cm thick aluminum. Two-bolt brackets join the columns and plates. The bolts are tightened to 14 Nm. Four Firestone Airmount isolators are bolted to the corners of the base plate. The isolators were inflated to 140 kPa and then individually adjusted such that the base of the frame was level and in line with a shaker used to provide excitation to the system.

The frame's natural frequencies and mode shapes were determined experimentally using a roving hammer impact test. Fifty-six impact locations were used with 7 reference accelerometers. An 8-channel, 24-bit Dactron system, laptop computer, and RT Pro SB v5.0 software were used. The data was analyzed using MEScopeVES, and 19 modes were found between 0 and 250 Hz.

A finite element model (FEM) of the frame was created using ABAQUS. This model was used to investigate the design of the auxiliary structures. Natural frequency and mode shape results of the FEM and modal test are compared in Table 1. The FEM predicted two modes not found in the modal test.

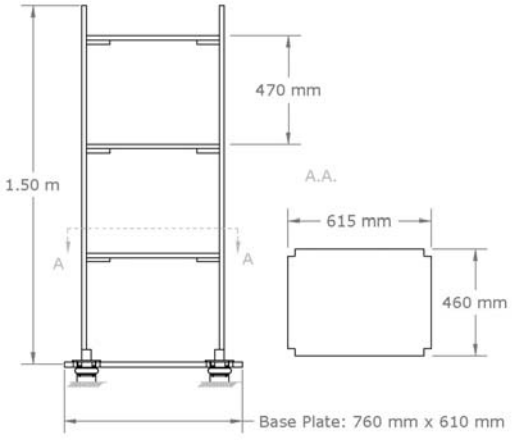

Figure 4: Schematic of moment resisting frame

Table 1: Model-test comparison of natural frequencies

Test Mode #	*Test (Hz)*	*FEM #*	*FEM (Hz)*	*% Error*
1	2.10	1	2.59	23.3
2	2.75	2	2.89	9.82
3	7.82	3	7.83	0.13
4	11.8	4	11.9	0.42
5	13.9	6	12.0	13.7
6	23.5	7	25.2	7.23
7	29.6	8	34.5	16.5
8	38.2	9	37.3	2.25
9	46.0	10	52.8	14.7
10	65.5	12	62.0	5.39
11	70.2	13	70.1	0.21
			mean %Error	8.51

All PZT patches used for testing were PSI-5H4E PZT from Piezo Systems Inc. The patches were cut to 32x72mm and attached using super glue. A vacuum application process was employed to ensure uniform pressure over the patch during glue curing.

The excitation force to the frame was provided using an electromagnetic shaker. The input signals were generated using RT Pro and amplified by a power amplifier. The frame structure was excited with a white noise signal. The Dactron system was used to measure the voltage output of the PZTs as well as the accelerometer outputs. The amplitude of the frame excitation signal remained constant for all tests. Because power harvesting involves very low levels of ambient vibration, it was assumed that both the frame and the auxiliary structure behave linearly.

4. TUNING PROCEDURE

The auxiliary structure was tuned to a resonant frequency of the frame structure. To ensure that all the low frequency modes of the frame were substantially excited, the shaker input was a broadband white noise. Also, the shaker was placed away from the nodes of the low frequency modes. The ambient excitation seen in real world applications does not exhibit the same uniform power spectrum, and may not excite all low frequency modes.

To optimize the energy input into the tuned auxiliary structure, the auxiliary structure should be placed at an anti-node, which is a location of maximum displacement for the particular mode that provides the most energy. This optimal location may not be known or may vary if the modal characteristics of the host structure change. Also, service and operational constraints may limit the possible locations of the auxiliary structure. Because practical location constraints are probable, the location of the auxiliary structure was arbitrarily chosen to be on the column between the first and second story. An acceleration frequency response function was recorded at the auxiliary structure point of contact, normal to the plane of the cantilever (Figure 5). The frequencies of the most dominant modes at that location were used to tune various auxiliary structures.

The auxiliary structure was tuned so that the frequency of its first bending mode would be equal to the frequency of the mode of interest. In the initial tuning iteration, the auxiliary structure was designed to have a first bending frequency slightly higher-than-optimum, so that it could be fine tuned by adding masses to the end of the beam. The first natural frequency of a slender cantilever beam with a concentrated end mass is given by [11]

$$\omega = \frac{1}{2\pi}\sqrt{\frac{3EI}{L^3(M+0.24M_b)}} \qquad (22)$$

Table 2 provides the geometric properties of the different auxiliary structures used during experimentation. All three auxiliary structures were made from aluminum and had an elastic modulus of 6.9E-10 Pa.

The auxiliary structure was mounted as shown in Figure 6. An accelerometer was placed near the clamp to measure the base excitation to the auxiliary structure. The accelerometer, PZT, and force transducer were connected to the Dactron analyzer to acquire frequency response functions (FRF's) from both the accelerometer and PZT. The FRFs were used to verify that the auxiliary structure was tuned.

For one of the auxiliary structures used, the resonant frequency of the host structure was at a distinctly different frequency than the first bending mode of the auxiliary structure as shown in Figure 7. To tune the auxiliary structure, a point-mass was added to the beam end. This mass was adjusted until the peaks of the auxiliary structure's resonant frequency and host structure's resonant frequency were of equal magnitude. Recall that a vibration absorber will split the frequency being damped into two new resonant frequencies, one higher and one lower in frequency than the original. This double-peak behavior can be seen in Figure 8. The output voltage of the PZT patch was maximized when the two frequencies were made to be as close as possible because at this point, the peak corresponding to the auxiliary structure was at its maximum.

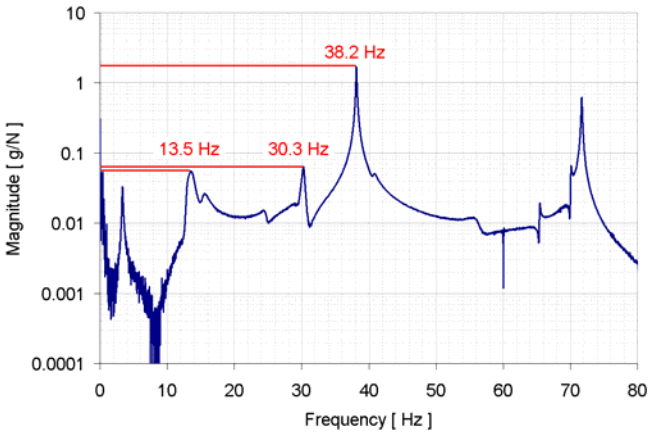

Figure 5: Acceleration FRF at the auxiliary structure mounting location

Table 2: Properties of auxiliary structure designs

	Length [mm]	*Width* [mm]	*Thickness* [mm]	*I* [m^4]
AUX 0	194	116	2.50	5.73E-11
AUX 1	153	34	1.25	5.53E-12
AUX 2	123	33	1.25	5.37E-12

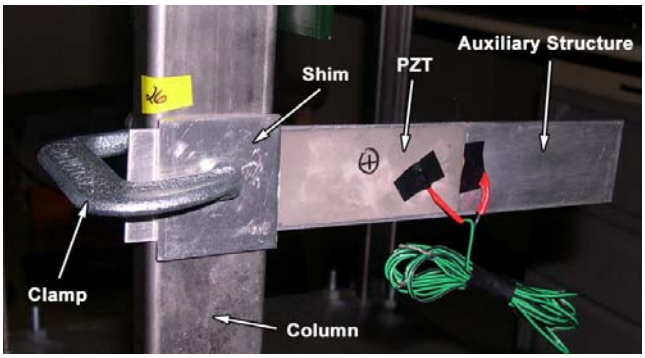

Figure 6: PZT and auxiliary structure mounting

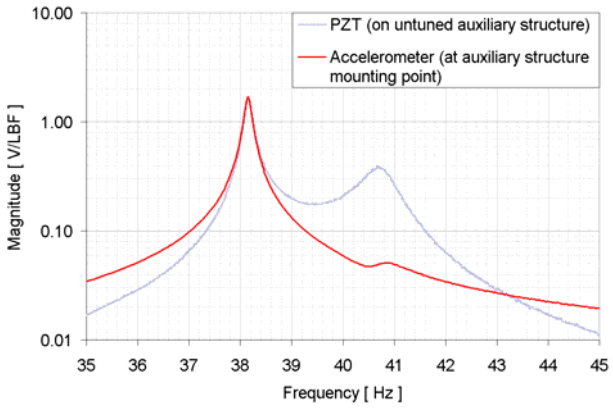

Figure 7: PZT and accelerometer frequency response functions at 38.2 Hz and 40.7 respectively

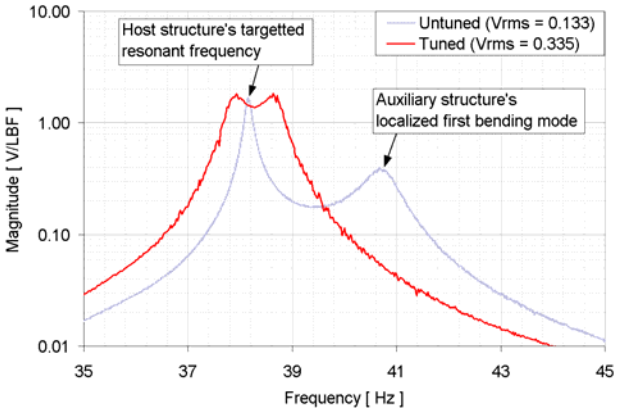

Figure 8: Frequency response function of tuned and mistuned auxiliary structures

When tuning the auxiliary structure, it was observed that the two frequencies remained distinct. The frequency corresponding to the auxiliary structure never matched that of the host structure. To examine this observation, the finite element model was used to vary the end mass in small increments and the two frequencies were plotted as a function of end mass as shown in Figure 9. An auxiliary structure was modeled in the FE software and attached to the model of the host structure. The auxiliary structure was modeled as a 162 mm long, 35 mm tall, and 1.4 mm thick shell element, and attached to the host structure model in a position and orientation emulating that of the experimental setup. The phenomenon of curve veering was observed. When curve veering occurs, the respective natural frequencies of the auxiliary structure and host will approach each other, and then diverge without ever crossing as shown in Figure 9 [15]. Another phenomenon associated with curve veering is mode switching. In Fig. 9 the "A" denotes that the natural frequency is associated with the auxiliary structure moving and the host structure being virtually stationary, while "H" corresponds to a mode where the host structure has significant motion. Note that as the end mass is increased, "A" switches from occurring at a higher frequency than "H" to a lower frequency than "H." When the two curves are close together, these modes become coupled and difficult to distinguish by shape.

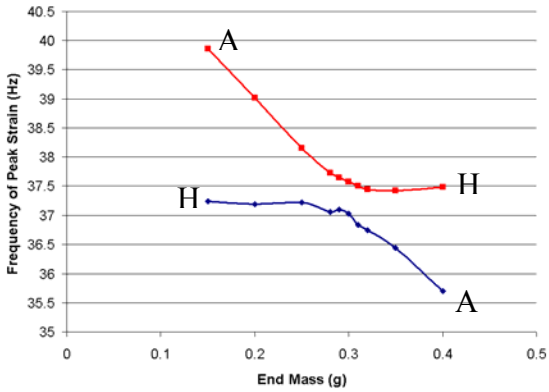

Figure 9: Illustration of curve veering.

For real applications it is important to understand how sensitive the voltage output is to tuning. Most notably, how precise does the tuning need to be and is the system susceptible to time variant modal characteristics. The FEM can be used to illustrate the importance of precise tuning of the auxiliary structure. The steady state analysis feature of ABAQUS was used to excite the model with sine waves of arbitrary but constant magnitude. These sine waves varied in frequency in discrete values for 35 Hz to 40 Hz. A modal damping factor of 1% of critical was included in the model. Strain at the base of the auxiliary structure was monitored. Figure 10 shows the effect of adjusting this mass on the resulting maximum strain value across the given frequency range. The peak strain is approximately two times greater at the tuned frequency than when mistuned by as little as 2 Hz. PZT voltage is proportional to strain, and electrical power is proportional to voltage squared, therefore power harvesting may potentially be improved significantly with precise auxiliary structure tuning. Unfortunately, this is highly susceptible to changes in the natural frequencies of the system. These frequencies could be perturbed over time in a real world system.

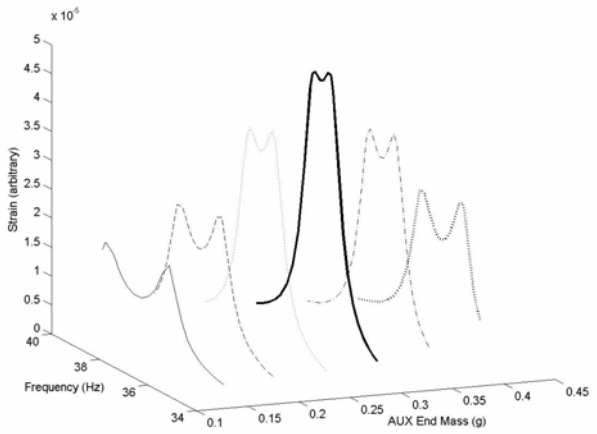

Figure 10: Strain at base of auxiliary structure for various end masses generated using the finite element model.

5. EXPERIMENTAL RESULTS

Quantifying the maximum energy harvesting capabilities of the auxiliary structure-mounted PZT required impedance matching. Impedance matching identifies the resistive load applied to the PZT needed for optimal power output. A potentiometer was used for varying load resistance. The auxiliary structure with mounted PZT was attached to the host structure. Impedance matching was conducted for both white noise and a sinusoidal force input (at the auxiliary structure's resonant frequency). If the PZT geometry remains constant for all samples, only

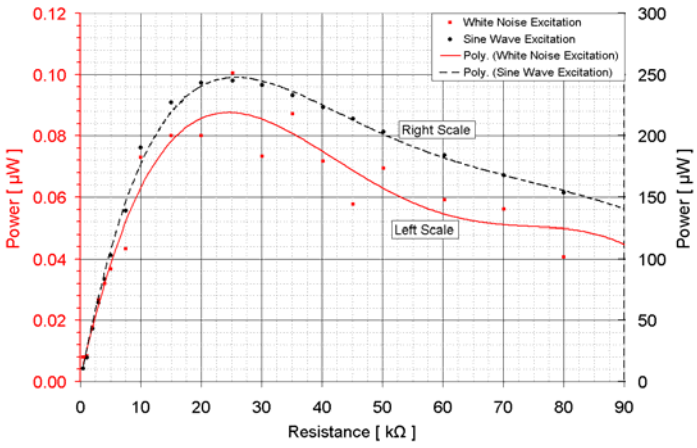

Figure 11: Impedance matching to determine the maximum power output.

one impedance matching procedure needs to be performed, and both white noise input and resonating sinusoidal excitation reveal identical optimum resistance. The only difference is in magnitude of the output level. This is illustrated in Figure 11. To generate this figure an auxiliary structure was attached to the host structure and the PZT was put into a resistive circuit. The resistance was varied, and for each resistance value, the rms voltage output of the PZT was recorded. The power was calculated using $P = V^2/R_L$, where P is the power output, V is equal to the rms voltage output of the PZT, and R_L is the resistive load. Note that the peak power output occurs approximately when R_L = 25 kOhms. Clearly from Figure 11 the power out when the system was forced at resonance with a sinusoidal signal was three orders of magnitude higher than when a low-level white noise input was used. The lower curve in Figure 11 uses the scale on the left side of the figure and the top curve uses the axis on the right side of the figure. The open loop voltage obtained for the low level random input was 0.108 V (rms) and the maximum power occurred at 0.050 V (rms). Theoretically, the maximum power output should occur at one half the open loop voltage [10], which was consistent with our results. From Figure 11 it is clear that the maximum amount of power that was harvested for this particular auxiliary structure was very small. When the base of the auxiliary structure underwent a $\pm$ 0.04 g acceleration range, the power output was on the order of 0.09 μW. Note that this acceleration range may not necessarily represent the acceleration ranges found in any particular real-world structure.

Tests on two different PZT patches in different configurations (one on the auxiliary structure and one on the host structure support column) revealed that the maximum power output occurred at the same resistive load, with only a difference in output magnitude. Since the primary objective of this study is to examine the use of auxiliary structures, and most notably tuned auxiliary structures for the improvement of power harvesting, for the remainder of this study we will only report open loop voltages. The open loop voltage should be directly related to the maximum output power since all the PZT patches used were identical.

Figure 12 shows the open circuit output voltage (rms) for a PZT glued to the column of the frame structure between the first and second story as well as the output voltage (rms) for a tuned and mistuned AUX 1 attached at the same location. The mistuned auxiliary structure had a natural frequency of 40.7 Hz, 2.5 Hz from the host structure's nearest mode at 38.2 Hz. AUX 1 was tuned to 38.2 Hz by attaching a point mass to the end of the beam as discussed in the previous section. A white noise force excitation was used, and output voltages were recorded for AUX 1. Figure 12 shows that the open loop voltage output increased by 130% when using an auxiliary structure, even one that is not precisely tuned. In this case, an additional 150% open loop output voltage gain can be achieved by tuning the auxiliary structure. The open loop voltage increased by almost a factor of 5 by using a tuned auxiliary structure rather than the host PZT. This indicated that the power would increase by a factor of approximately 25.

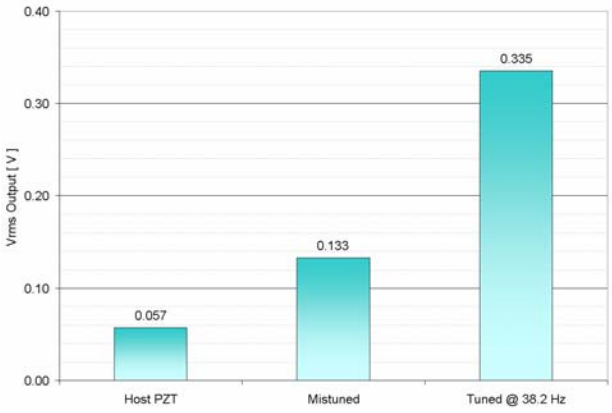

Figure 12: Voltage output improvement using a tuned and mistuned auxiliary structure.

From Eq. (21), the magnitude of the host's mode shape at the location of the auxiliary structure is an important factor to consider when choosing the mode for which to tune. Higher output voltages should be achieved by attaching the PZT to an auxiliary structure that is tuned to a well-excited mode. To determine which host structure mode to tune for, two factors must be considered: (1) the host structure force input, that is, how well does it excite a particular mode, and (2) the location of the auxiliary structure, that is, the magnitude of the mode at that location. As explained in the test setup section, the frame structure was excited using white noise, a random signal with a uniform power spectrum. To examine the effect of tuning to different modes, AUX 1 was tuned to the 38.2 Hz mode and AUX 2 was tuned to the 71.6 Hz mode of the host structure. The auxiliary beams were mounted at an anti-node of the respective host structure mode shape, and the magnitude of the mode shapes were approximately the same at these locations. The PZT patches on the 38.2 Hz and on the 71.6 Hz tuned beams both generated approximately 0.33 volts rms. Had a forcing function with a non-uniform power spectrum been used, the modes would likely not have been excited to the same degree, and the PZTs on the auxiliary structures would have generated different voltages.

To optimize the energy input to the tuned auxiliary structure, the beam should be placed at an anti-node for the particular mode that is excited the most, as done in the above experiment. In reality, this optimal location may not be known or may change if the modal characteristics of the host structure change. Also, service and operational constraints may limit the possible locations of the auxiliary structure. Because practical location constraints are probable, the location of the auxiliary structure was arbitrarily chosen to be on the column between the first and second story. From the acceleration FRF recorded at the auxiliary structure's point of contact, normal to the plane of the cantilever (Figure 5), the most dominant modes were the 38.2 Hz and the 71.6 Hz modes. Due to geometric constraints of the beam, the auxiliary structure could only be tuned to a small frequency band. For this reason, the 38.2 Hz, 30.3 Hz, and 13.5Hz modes were used to tune AUX 1.

Eq. (21) suggests that the mode with the highest acceleration force response for a given location and force input will provide the greatest excitation to the auxiliary structure and the highest output voltage. The 38.2 Hz mode had a much larger peak in the FRF than the 13.5 Hz and 30.3 Hz modes, and thus was expected to have a much larger open loop voltage. This analytical result was verified by the experimental findings as shown in Figure 13. The open circuit voltage outputs were collected while the frame was excited with a white noise shaker input. The 38.2 Hz mode provided over 3.5 times the PZT voltage output than the other frequencies. It is important to note that the 13.5 Hz and 30.3 Hz modes do not follow the relationship in Eq. (22). The 30.3 Hz mode has a larger FRF peak than the 13.5 Hz mode; however, the 13.5 Hz mode has a larger voltage output. This discrepancy may be attributed to the small variance between the FRF magnitudes; the 30.3 Hz mode is only slightly larger than the 13.5 Hz mode. Also, the 30.3 Hz mode required a 6.25 gm point mass addition to tune while the 13.5 Hz mode required a 35.0 gm point mass addition to tune. This larger mass at the tip of the auxiliary structure will obviously influence the strain at the base of the auxiliary structure and therefore the output voltage of the PZT. Eq. (21) was derived for a uniform cantilever beam vibrating in its first mode and not one with a point mass.

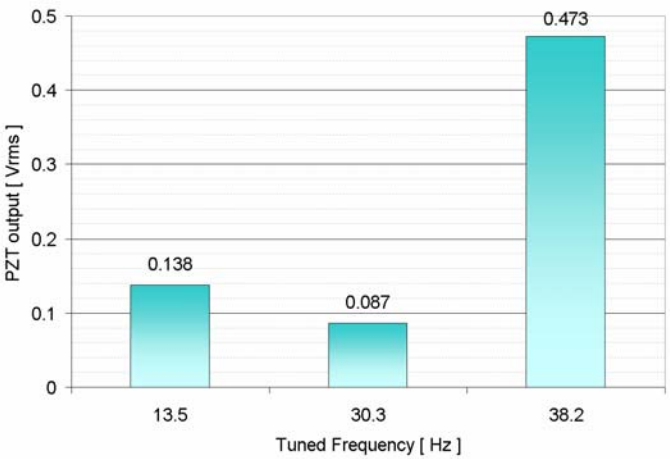

Figure 13: Voltage output sensitivity to tuning mode

6. CONCLUSION

This paper presents an approach for improving PZT power output from a vibrating structure by using a tuned auxiliary structure. A theoretical equation was developed to ascertain the important parameters to consider when designing a tuned auxiliary structure, and a method of tuning the auxiliary structure was presented. The following conclusions can be drawn from this study:

1. An auxiliary structure, even if mistuned, can enhance power harvesting.
2. Tuning the auxiliary structure can significantly improve power generation.
3. The PZT power output is very sensitive to tuning. To reap the benefit of tuning, the auxiliary structure must be accurately tuned. Also, the system is susceptible to operational changes in mode characteristics.
4. Depending on the force input, the modes of the host structure will be excited differently. Given the realistic, operational force input, the frequency of the most dominant mode should be used to tune the auxiliary structure.
5. It is optimal to place the auxiliary structure at an anti-node, that is, at the location of maximum displacement of the mode for which the auxiliary structure is tuned. If the anti-node is unknown, or there are operational constraints, this will control the placement location of the auxiliary structure. The mode with the dominant frequency response at a particular location should be used for tuning.

During experimentation, the end mass was used to tune the auxiliary structure to the desired frequency. It is believed that these added masses, which ranged as high as 35.0 gm, affected the results. This end mass was not accounted for in the developed theory. For future work this end mass must be accounted for in the theory or removed from the experimental design.

7. ACKNOWLEDGMENTS

The authors would like to thank the Engineering Science and Applications Division at the Los Alamos National Laboratory as well as the Department of Energy's Education Programs office for funding for the Los Alamos Dynamics Summer School. Appreciation is also expressed to the following companies that provided the software packages that facilitated this research:

- Vibrant Technologies (MEScopeVES experimental modal analysis software)
- The Mathworks, Inc. (MATLAB numerical analysis software)
- Hibbitt, Karlsson and Sorensen, Inc. (ABAQUS finite element software).

8. REFERENCES

[1] Chadrakasan, A., Amirtharajah, R., Goodman, J., Rabiner, W. "Trends in Low Power Digital Signal Processing," *International Symposium on Circuits and Systems,* pp. 604-607, 1998.

[2] Farrar, C.R., et. al. "Damage Prognosis: Current Status and Future Needs," Report LA-14051-MS, Los Alamos National Laboratory, 2003.

[3] Sodano, H., E. A. Magliula, G. Park, D. J. Inman, "Electric Power Generation using Piezoelectric Devices," *Proceedings of 13th International Conference on Adaptive Structures and Technologies,* October 7-9, Berlin, Germany, 2002.

[4] Sodano. H., G. Park, D. J. Leo, D. J. Inman, "Use of Piezoelectric Energy Harvesting Devices for Power Storage in Batteries," *Proceedings of 10th SPIE Conference on Smart Structures and Materials*, March 2-6, San Diego, CA, 2003.

[5] Fry, D., Holcomb, D., Munro, J., Oakes, L., Maston, M. "Compact Portable Electric Power Sources" Report ORNL-TM-13360, Oak Ridge National Laboratory, 1997.

[6] Starner, T., "Human-powered Wearable Computing," *IBM Systems Journal*, Vol 35, pp.618, 1996.

[7] Elvin, N., Elvin, A., Choi, D H. "A Self-Power Damage Detection Sensor". J. Strain Analysis, Vol. 38 No. 2, p.115-124, 2003.

[8] Elvin, N.G., A. Elvin, M. Spector,"A Self-powered Mechanical Strain Energy Sensor," Smart Materials and Structures, 10, pp. 293-299, 2001.

[9] Roundy, S., Wright, P., Rabaey, J. "A Study of Low Level Vibrations as a Power Source for Wireless Sensor Nodes". Computer Communications, Vol. 23, p.1131-1144, 2003.

[10] Ottman, G.K., H. F. Hofmann, A. C. Bhatt, "Adaptive Piezoelectric Energy Harvesting Circuit for Wireless Remote Power Supply," IEEE Transactions on Power Electronics, Vol 17, No. 5, Sept. 2002.

[11] Ottman, G.G,k H.F. Hofmann, G.A Lesieutre, "Optimized Piezoelectric Harvesting Circuit Using Step-Down Converter in Discontinuous Conduction Mode," IEEE Transactions on Power Electronice, Vol 18, No. 2, Mar. 2003.

[12] Application Data. 1 Jan 2003. Piezo Systems. 16 May 2003 <http://www.piezo.com/appdata.html>

[13] Ugural, A., Fenster, S., Advanced Strength and Applied Elasticity. New Jersey: Prentice Hall PTR, 1995.

[14] Blevins, R., Formulas for Natural Frequency and Mode Shape. Florida: Kriefer Publishing Co., p. 158, 1995.

[15] Perkins, N.C., C.D. Mote, "Comments on Curve Veering in Eigenvalue Problems," Journal of Sound and Vibration, Vol. 106, No. 3, pp. 451-463, 1986.